Current Biology

CellPress

Report

A novel nabelschnur protein regulates segregation of the kinetoplast DNA in *Trypanosoma brucei*

Lawrence Rudy Cadena,[1,4,5,7,*] Michael Hammond,[1,2,4,*] Martina Tesařová,[1] Ľubomíra Chmelová,[3] Michaela Svobodová,[1] Ignacio M. Durante,[1,6] Vyacheslav Yurchenko,[3] and Julius Lukeš[1,2]

[1]Institute of Parasitology, Biology Centre, Czech Academy of Sciences, České Budějovice (Budweis) 370 05, Czech Republic
[2]Faculty of Sciences, University of South Bohemia, České Budějovice (Budweis) 370 05, Czech Republic
[3]Life Science Research Centre, Faculty of Science, University of Ostrava, Ostrava 701 03, Czech Republic
[4]These authors contributed equally
[5]Present address: Institute of Microbial Cell Biology, Heinrich Heine University, Düsseldorf 40225, Germany
[6]Present address: George Washington University, Washington, DC 20052, USA
[7]Lead contact
*Correspondence: lawrence.cadena@hhu.de (L.R.C.), michael.hammond@paru.cas.cz (M.H.)
https://doi.org/10.1016/j.cub.2024.08.044

SUMMARY

The acquisition of mitochondria was imperative for initiating eukaryogenesis and thus is a characteristic feature of eukaryotic cells.[1,2] The parasitic protist *Trypanosoma brucei* contains a singular mitochondrion with a unique mitochondrial genome, termed the kinetoplast DNA (kDNA).[3] Replication of the kDNA occurs during the G_1 phase of the cell cycle, prior to the start of nuclear DNA replication.[4] Although numerous proteins have been functionally characterized and identified as vital components of kDNA replication and division, the molecular mechanisms governing this highly precise process remain largely unknown.[5,6] One division-related and morphologically characteristic structure that remains most enigmatic is the "nabelschnur," an undefined, filament-resembling structure observed by electron microscopy between segregating daughter kDNA networks.[7–9] To date, only one protein, TbLAP1, an M17 family leucyl aminopeptidase metalloprotease, is known to localize to the nabelschnur.[9] While screening proteins from the *T. brucei* MitoTag project,[10] we identified a previously uncharacterized protein with an mNeonGreen signal localizing to the kDNA as well as forming a point of connection between dividing kDNAs. Here, we demonstrate that this kDNA-associated protein, named TbNAB70, indeed localizes to the nabelschnur and plays an essential role in the segregation of newly replicated kDNAs and subsequent cytokinesis in *T. brucei*.

RESULTS

TbNAB70 localizes to the kDNA and nabelschnur, exhibiting cell-cycle-specific expression

TbNAB70 (Tb927.11.7580) is a basic (pI 9.18), 70 kDa hypothetical protein with a predicted N-terminal mitochondrial targeting sequence. When screening for proteins exhibiting a distinct kinetoplast signal through the MitoTag project,[10] TbNAB70 was identified as warranting further scrutiny.

To verify whether TbNAB70 represented a genuine kinetoplast DNA (kDNA) component, we endogenously tagged its C terminus with a $V5_{\times 3}$ epitope in SmOx procyclic stage of *T. brucei*.[11,12] Co-localization with DAPI confirmed that TbNAB70 localizes to the kDNA in the G_1 phase, before progressing into early 1Kdiv1N cells (1 dividing kDNA alongside 1 nucleus) to a dumbbell-like structure co-localizing with the kDNA discs (Figure 1A; Figure S1). Shortly afterward, the discs commence segregation into the daughter kDNA networks positioned perpendicular to one another.

At this stage, the characteristic nabelschnur between the newly replicated kDNA becomes apparent throughout the TbNAB70 signal (Figure 1A). As the daughter kDNA discs progressively separate (2K1N stage, note the apparent lack of the DAPI signal in the space between them), the nabelschnur remains continually present (Figures 1A and 1B). Nabelschnur disintegration begins only at distances greater than approximately 2 μm between the daughter kDNAs during the 2K1N phase, when the TbNAB70 signal remains confined to two regions overlaying each newly synthesized kDNA disc (Figure 1C). Of note, the fluorescent intensity increases when the nabelschnur is present and diminishes once the structure disappears at the 2K1N phase (Figure 1D), strongly suggesting that the level and distribution of TbNAB70 is phase specific. To explicitly verify $TbNAB70_{V5}$ localization, we employed immunodecoration of cryosectioned cells processed for transmission electron microscopy using gold-labeled α-V5 antibody. We documented gold particles on the periphery of the electron-dense kDNA disc, showing greater accumulation on its apical side, in addition to areas where the nabelschnur is localized (Figure 1E). Therefore, we conclude that TbNAB70 dually localizes to the nabelschnur and the kDNA periphery and exhibits cell-cycle-specific expression.

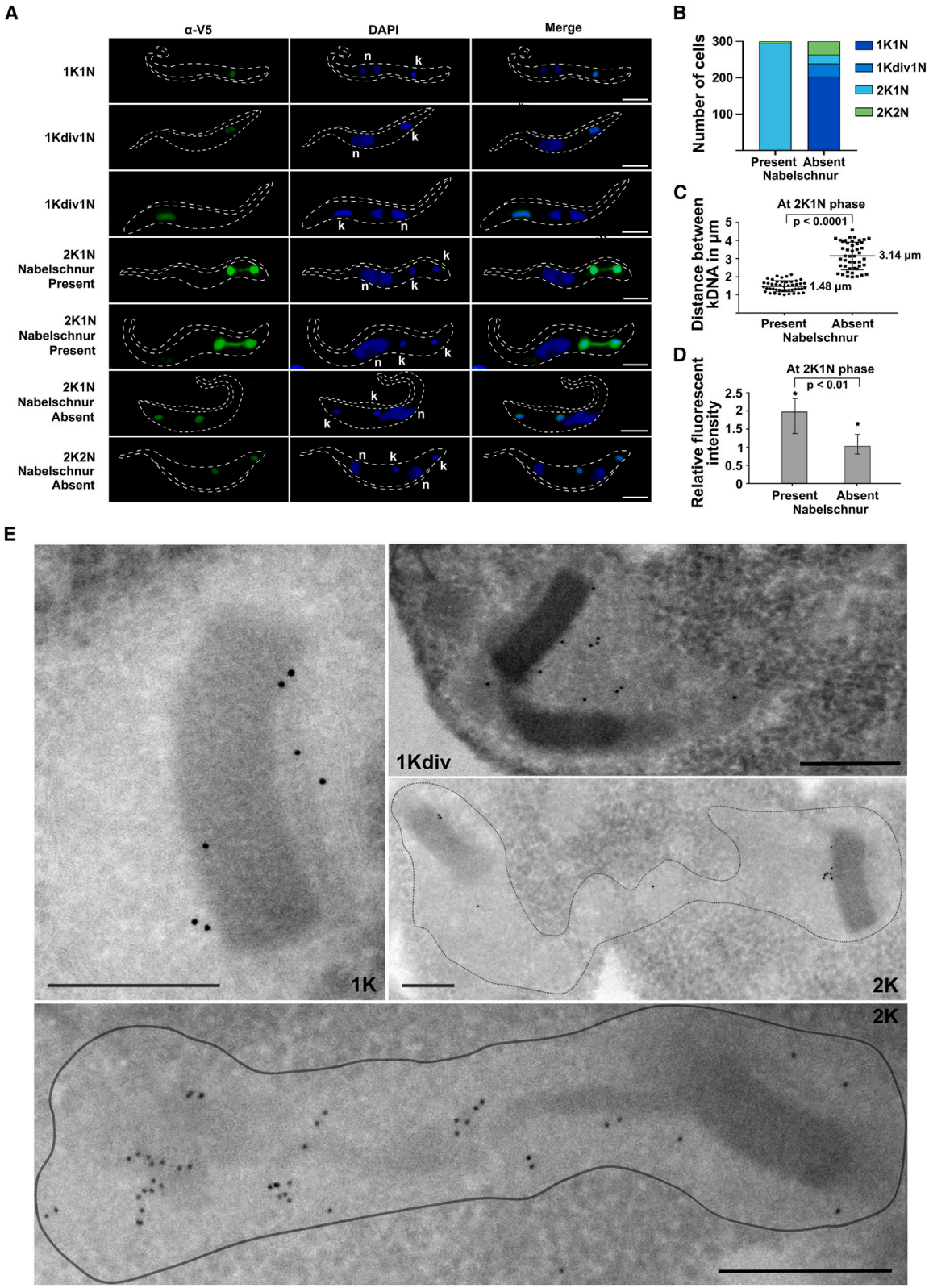

Figure 1. Localization of TbNAB70 in procyclic *T. brucei*

(A) Representative immunofluorescence microscopy images of $TbNAB70_{V5}$ procyclic cells during different phases of the cell cycle (1K1N, 1Kdiv1N, 2K1N, and 2K2N). $TbNAB70_{V5}$ (green) was detected by α-V5 antibody. The kDNA (k) and the nucleus (n) were stained with DAPI (blue). Scale bars: 2 μm. See also Figure S1.

(legend continued on next page)

Depletion of TbNAB70 demonstrates an essential function in kDNA segregation and cytokinesis

To study TbNAB70's function, we depleted the corresponding mRNA by RNA interference (RNAi) using a tetracycline-inducible vector[13] in our TbNAB70$_{V5}$ cell line. The RNAi knockdown was efficient, as probing for TbNAB70$_{V5}$ in western blots showed ablation by 48 h post RNAi induction (Figure 2A). The cells displayed a severe growth defect within 24 h post RNAi, indicating that this protein is critical for cell viability (Figure 2B). MitoTracker red staining of induced cells revealed neither morphological defects of the mitochondrion nor the loss of its membrane potential (Figure 2C). To investigate cytokinesis-related phenotypes, we performed DAPI counts on cells before treatment as well as following RNAi induction (Figure 2D). Cells exhibiting a 1K1N (G_1 phase) phenotype decreased from approximately 65% non-induced to 53% and then 40% at 24 and 48 h post RNAi, respectively (Figure 2E). Additionally, we recorded that ∼15% of cells undergoing TbNAB70 knockdown depicted an aberrant 1K2N phenotype at 24 h, increasing to ∼25% at 48 h. This 1K2N phenotype was lacking in non-induced cells, indicating abnormalities in both kDNA segregation and cell cycle upon depletion of TbNAB70. Interestingly, 10% of cells showed 1Kdiv2N (1 dividing kDNA alongside 2 nuclei) 24 h post RNAi, although this later decreased to 5%. Moreover, a similar decrease was observed for cells exhibiting 2K1N and 2K2N phenotypes. No zoids (cells containing kDNA, but lacking a nucleus) were observed.

Next, we examined whether TbNAB70 depletion alters the abundance of kDNA minicircles and/or maxicircles, potentially indicating a function in kDNA replication. We employed Southern blot analysis of total DNA isolated from trypanosomes 0, 24, and 48 h post RNAi induction, in addition to wild types, using specific probes against minicircles and maxicircles, with tubulin serving as a loading control. The lack of change in their gross abundance following TbNAB70 depletion (Figure 2F) suggests that kDNA replication itself is not affected when normalized to total DNA amount in a pool of cells during different cell-cycle stages. However, this method cannot distinguish whether kDNA replication has taken place in cells where one kDNA is present alongside two nuclei (1K2N phenotype). To determine whether kDNA has indeed replicated, but not separated in cells during this phase, we quantified the DAPI intensity of the kDNA in individual cells showcasing the 1K1N phenotype and compared it to that found within 1K2N cells. A near-2-fold increase in kDNA intensity for these cells (Figure 2G) indicates that the kDNA had approximately doubled yet had not segregated. To assess the catenation for this unsegregated kDNA network, we isolated kDNA from 0- and 48-h-post-RNAi-induction cells, which underwent separation via electrophoresis. The large kDNA catenane migrated only minimally in both samples; however, two smaller, faint bands were visible only in the 48-h lane (Figure S2). These ∼1.0- and >15.0-kb bands correspond to the sizes of free minicircles and maxicircles, respectively, indicating that this unsegregated kDNA, accumulating in 1K2N cells, is not completely re-catenated, suggesting specific functional importance of TbNAB70.

To determine whether TbNAB70 depletion influenced the abundance of the tripartite attachment complex (TAC) or other kinetoplast-associated proteins, we performed quantitative proteomics comparing non-induced cells and those 48 h post RNAi (Figure 2H). We observed no significant changes in the cohort of kDNA replication and associated factors, save for a 2.72-fold decrease in levels of POLIC, a protein suggested to play a role in maxicircle replication that dually localizes to the kinetoflagellar zone (KFZ) and the antipodal sites (APSs).[14,15] It is worth noting that three components of the TAC also displayed significant changes in their expression levels, most prominently TAP110 (Tb927.11.7590) and an undescribed TEX-like protein (Tb927.11.6660), which were both upregulated 9.15- and 3.84-fold, respectively. Such an increase (in comparison to other TAC components) is of particular interest, as the overexpression of TAP110 led to a strong increase of Tb927.11.6660,[16] indicating that these two proteins may form a yet-undescribed interaction. Furthermore, TAP110, known to play a supporting role in the separation of replicated kDNA networks,[16] is present directly upstream of TbNAB70 within the genome of *T. brucei*. By contrast, there was a decrease in the level of p166, another characterized TAC protein.[17] Beyond the kDNA and TAC components, we noted a strong decrease (−9.58-fold) of basal body protein SAS6 and, to a lesser degree, two proteins of the flagellar attachment zone (FAZ) (of a total 46 known FAZ proteins). Additionally, we witnessed significantly reduced levels of 35 proteins of the large and small subunits of mitochondrial ribosomes and upregulated levels of kinetoplast ribosomal pentatricopeptide proteins (KRIPPs)[18] (Figure 2H; Data S1A and S1B).

Proteomics data of TbNAB70 RNAi cells suggested prominent depletion of the FAZ and basal body components (Figure 2H). Accordingly, we sought to visualize changes in these regions using antibodies against FAZ1 and YL1/2, the latter being a marker for the mature basal bodies. The 1K2N cells at 48 h post RNAi displayed a single FAZ signal, indicating an inability to synthesize a second FAZ. No second flagellum was apparent, and approximately 22% of 1K2N cells were observed with a detached primary flagellum, accompanied by aberrant cell morphology. Most of these cells additionally lacked a second mature basal body, with only 13% of cells showing a distinct second signal (Figure 2I), instead displaying a singular signal that appeared brighter and elongated when compared with that observed in recently divided 1K1N cells. Together, this demonstrates that depletion of TbNAB70 impedes basal body segregation, but

(B) Graph depicting presence and absence of TbNAB70$_{V5}$-visualized nabelschnur during specific phases of the cell cycle. 100 cells were counted at random with three biological replicates (n = 3), resulting in a total of 300 cells represented on the graph.
(C) Quantitative analysis of distance between two daughter kDNA networks during 2K1N phase measuring length when the nabelschnur disappears.
(D) Relative fluorescent intensity of TbNAB70$_{V5}$ signal associated to the kDNA during 2K1N phase while the nabelschnur is present or absent. Forty cells were measured with both nabelschnur present and absent, with the average intensity of green fluorescence seen in the nabelschnur-lacking 2K1N cells set to 1 as a value. Asterisks show maximum value.
(E) Transmission electron microscopy for cryosections of TbNAB70$_{V5}$ cells immunolabeled with protein A (10 nm). Drawn lines indicate mitochondrial periphery. Note the visible nabelschnur in the bottom figure. Scale bar: 250 nm.

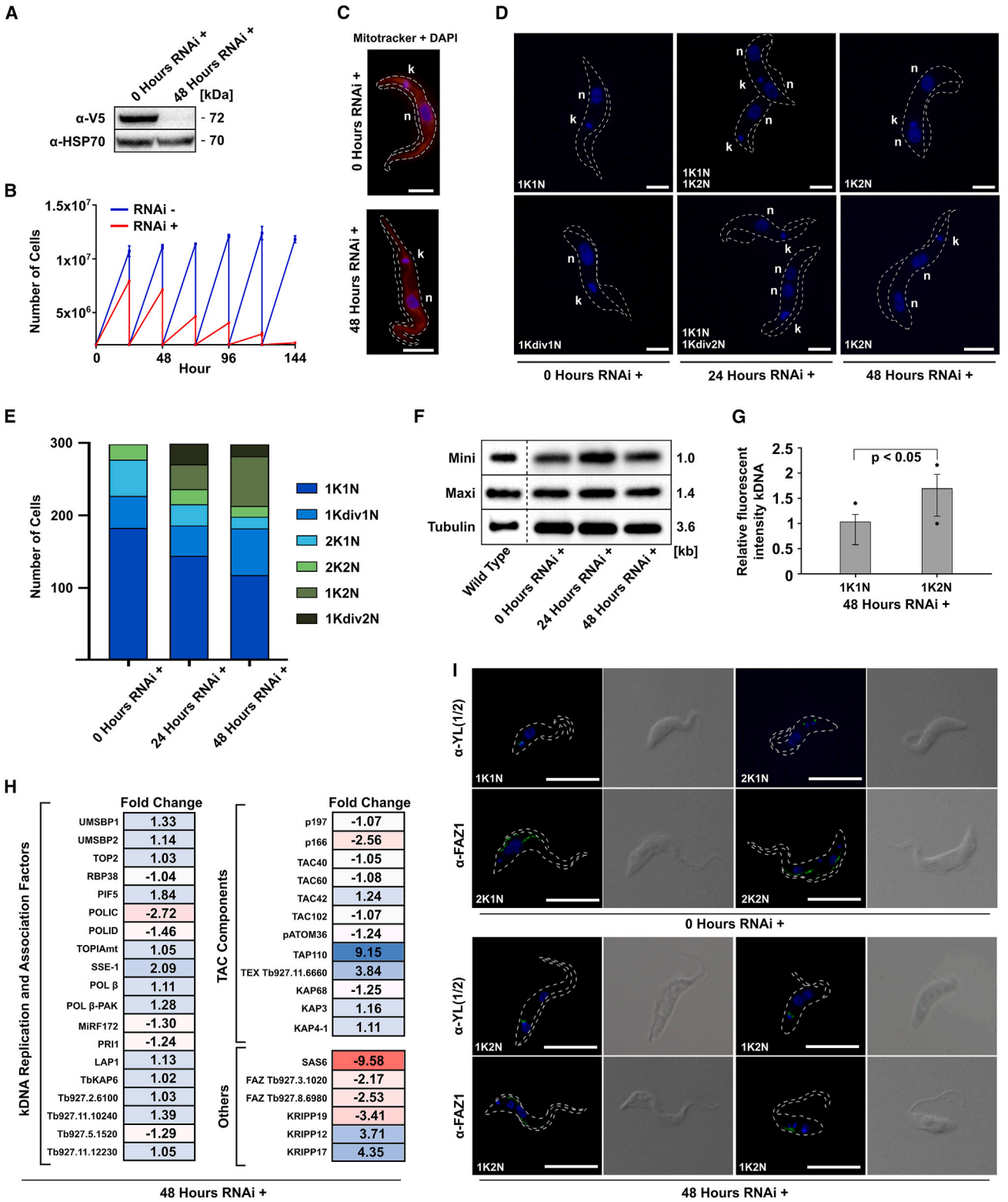

Figure 2. Depletion of TbNAB70 mRNA by RNAi

(A) Western blot of whole-cell lysates showing complete depletion of TbNAB70$_{V5}$ at 48 h post RNAi induction. TbNAB70$_{V5}$ was detected by α-V5 antibody. Heat shock protein 70 (HSP70) served as a loading control.

(B) Growth curve of non-induced and RNAi-induced TbNAB70$_{V5}$ cells (n = 3, mean and standard deviation values are shown).

(legend continued on next page)

not necessarily maturation, as well as the generation of a second FAZ. In turn, electron microscopy analysis of this RNAi cell line displayed a greater abundance of trypanosomes (6/20 cells observed compared with none observed in the uninduced line) with a denser kDNA disc and two unsegregated mature basal bodies, suggestive of the arrested state of these 1K2N cells (Figure S3).

In silico structural analysis of TbNAB70 indicates a potential capacity for kDNA binding

In addition to an N-terminal target sequence of 23 amino acids, hits for a coiled-coil domain (278–306) as well a C-terminal intrinsically disordered domain were identified (Figure 3A). Although no homologous proteins encompassing the entirety of TbNAB70 were detected, one particular region (382–484) showed homology to various mitochondrial-DNA-binding proteins (Table S1), such as Gcf1p of *Candida albicans*, containing high-mobility group (HMG) box domains.[19]

AlphaFold2 analysis of TbNAB70's tertiary structure revealed 6 (3 + 3) small α helices confined in triangular spaces between amino acids 386–421 and 433–480 (Figures 4A and 4B). Because these motifs are hallmarks of the HMG box domains,[20,21] we term them HMG boxes 1 and 2, which are confidently predicted by AlphaFold2 (90 > pLDDT > 70) (Figure 4C). Additionally, the coiled-coil domain showed the highest confidence (pLDDT > 90), while the predicted intrinsically disordered region at the C terminus showed very low confidence (pLDDT < 50), typical for predicted disordered regions.[22]

TbNAB70 is restricted to parasitic kinetoplastids and likely developed in tandem with *TAP110*

We investigated the phylogenetic distribution of *TbNAB70* within a spread of available genomes and transcriptomes for representatives of the phylum Euglenozoa in comparison to the only other characterized nabelschnur protein, TbLAP1 (Figure 3D).[9] Similarly, we opted to assess the TAC components TAP110 and Tb927.11.6660, which displayed notable enrichment following TbNAB70 RNAi.

Of the two identified nabelschnur components, *TbLAP1* shows conserved distribution in all surveyed kinetoplastid flagellates, with homologs present in other Euglenozoa and likely beyond (Figure 3D). Conversely, *TbNAB70* is confined to Trypanosomatidae, a clade of exclusively parasitic kinetoplastids. Despite their co-enrichment, genes for TAC components TAP110 and Tb927.11.6660 show contrasting levels of distribution, with *Tb927.11.6660* present in the majority of Euglenozoa, while *TAP110* shows a highly complementary distribution to that of *TbNAB70*, suggesting a similar time of emergence for these two proteins. Shared synteny is seen in all four proteins throughout the genus *Trypanosoma*,[23] while additionally being broadly present in the clade of Leishmaniinae as well as in the early-branching *Paratrypanosoma confusum*, except for *TAP110* (Figure 3D). Such a discrepancy is notable, considering that *TAP110* and *TbNAB70* are neighboring genes, suggesting a break in this syntenic region occurring immediately upstream of *TAP110* in the common ancestor of this clade. *TbNAB70* is absent from *Vickermania ingenoplastis* and shows a lack of synteny for all other surveyed genes in this study, indicating a high level of gene movement and disruption in this organism. *TAP110* has additionally been lost in *Angomonas deanei*, while both genes are absent from *Novymonas esmeraldas*, which prompts speculation on these organisms' execution of kDNA segregation.

DISCUSSION

Until now, TbLAP1 represented the only identified protein that localized to the nabelschnur, the final physical connection between two dividing daughter kDNA discs during cytokinesis of *T. brucei*.[9] Here, we report the identification of TbNAB70, a second protein localizing to the nabelschnur as well as the kDNA periphery. Expression of TbNAB70 appears cell-cycle specific from our analysis, demonstrating greater abundance during kDNA division compared with G_1 (Figures 1A and 1B). This is in agreement with previous work, in which stability of the TbNAB70 transcript peaked during the S phase, where the basal bodies and kDNA daughter networks undergo segregation (Figure S4).[24] Although the knockdown of TbLAP1 results in an accumulation of 2K2N cells, delayed cytokinesis, and lower growth rate, it is not lethal.[9] By contrast, TbNAB70 knockdown displayed a drastic growth defect accompanied by an accumulation of 1K2N cells, possessing replicated kDNA but with incomplete catenation, being unable to segregate. Furthermore, these cells typically fail to separate the basal bodies and manifest a second

(C) Immunofluorescence images of non-induced cells (0 h RNAi+) and induced cells (48 h RNAi+) stained with MitoTracker Red (red), with kDNA networks (k) and nuclei (n) as detected as in Figure 1. Scale bar: 2 μm.

(D) Representative immunofluorescence images of non-induced cells (0 h RNAi+) and induced cells (24 h RNAi+ and 48 h RNAi+) depict kDNA networks (k) and nuclei (n) as quantified in (E).

(E) Quantification of the relative occurrence of kDNA networks and nuclei in the non-induced cells (0 h RNAi+) and induced cells (24 h RNAi+ and 48 h RNAi+). 100 cells were chosen at random and analyzed. Three biological replicates were performed (n = 3), resulting in a total of 300 cells depicted on the graph. Mean and standard deviation values are shown.

(F) Southern blot analysis of wild-type, non-induced cells (0 h RNAi+) and induced cells (24 h RNAi+ and 48 h RNAi+). Numbers indicate size of DNA fragments in kb.

(G) Relative fluorescent intensity of DAPI-stained kDNA in 48-h-RNAi-induced cells. kDNA intensity was measured in 20 cells depicting the phenotype 1K1N and compared with kDNA intensity of 20 cells depicting the phenotype 1K2N. The average intensity of kDNA in the 1K1N cells was normalized to 1 as a set value. Asterisks show maximum and minimum values. Mean and standard deviation data are shown. See also Figure S2.

(H) Heatmap showing increase or decrease in fold change in selected proteins encompassing kDNA replication and associated factors, TAC components, and other proteins of interest in cells 48 h post induction (in triplicate). For the full list of proteins identified, see Data S1A. For list of proteins with significant values, see Data S1B.

(I) Immunofluorescence images of non-induced cells (0 h RNAi+) and induced cells (48 h RNAi+). Mature basal body stained with α-YL1/2 (green) or flagellum stained with α-FAZ1 (green). Scale bar: 10 μm. Note the detachment of the flagellum on the bottom right image. See also Figure S3.

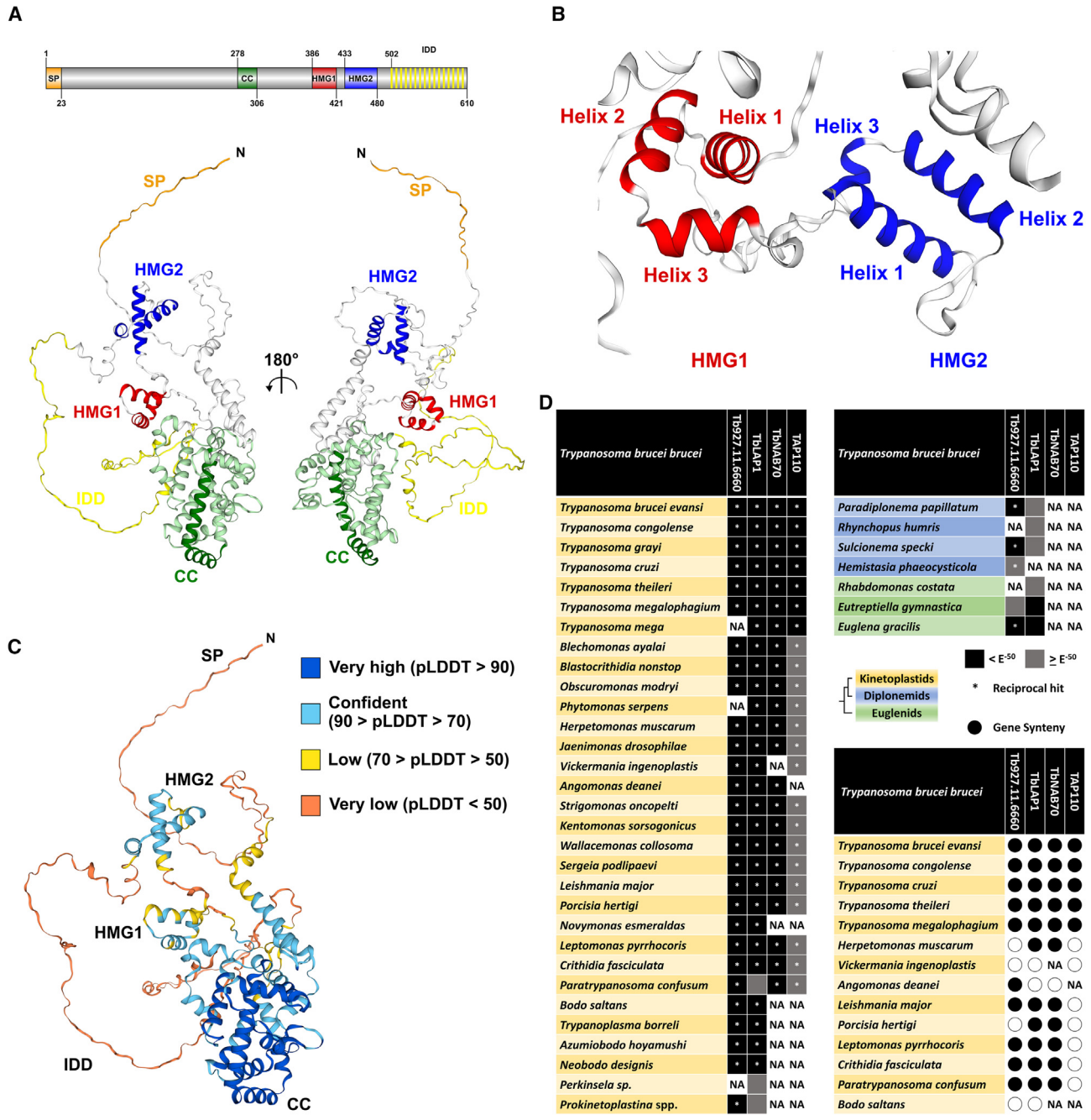

Figure 3. *In silico* analysis of TbNAB70 and phylogeny of associated proteins

(A) AlphaFold2 structure of TbNAB70. Predicted signal peptide (SP) is in orange, coiled-coil (CC) domain in dark green, regions of highest confidence in light green on tertiary structure, high-mobility group box 1 (HMG1) in red, high-mobility group box 2 (HMG2) in blue, and predicted intrinsic disordered domain (IDD) in yellow. The linear map of the domains is shown above. For HHPred results, see Table S1.

(B) Close-up view of tertiary structure of HMG box 1 and HMG box 2.

(C) Gross confidence scores from AlphaFold2.

(D) Presence and conservation of TbNAB70 and relevant genes (TbLAP1, TAP110, and TEX-like-Tb927.11.6660) across the Euglenozoan phylum with hit thresholds lower than E^{-50} indicated in black and greater in gray. Assessment of synteny across high-quality genomes of Trypanosomatidae, empty circles indicate a lack of gene synteny with *T. brucei*, sequence information available in Table S2. See also Figure S4.

FAZ, which is consistent with TbNAB70's peak expression in the S phase, when kDNA replication and basal body segregation occur (kDNA replication and probasal body maturation occur previously during the late G_1 phase, while new FAZ formation occurs in the succeeding G_2/M phase) (Figure S4). It has been proposed that the newly formed FAZ from the elongation of the

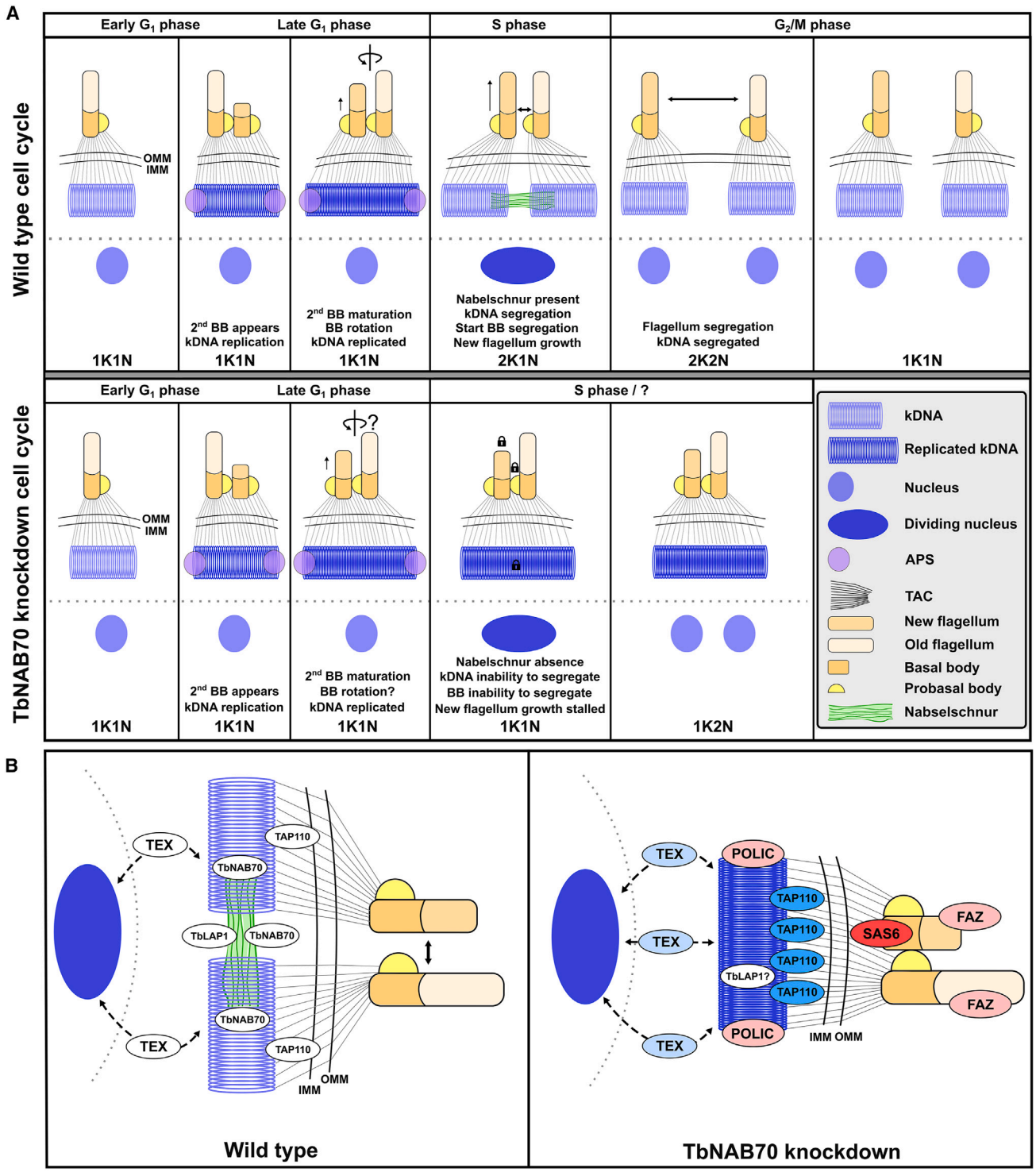

Figure 4. Mechanism of action model of TbNAB70-dependent kDNA segregation

(A) Model of the proposed mechanism of replicated daughter kDNA segregation throughout the *T. brucei* cell cycle. OMM marks the outer mitochondrial membrane and IMM is the inner mitochondrial membrane.

(B) Model of interactions for selected kinetoplast and flagellum-associated proteins, either enriched (blue) or depleted (red) by TbNAB70 knockdown.

emerging flagellum influences the correct formation of the division furrow between the separated basal bodies during cytokinesis.[25] Interestingly, depletion of the basal body protein TbCentrin4 does not affect FAZ levels or flagellum assembly,[26] resulting in cases where the daughter cells inherit either 2 nuclei or none. The opposite appears to occur in the absence of TbNAB70, where there is an inability to complete a full-length second flagellum in addition to the basal bodies being unable to segregate, resulting in a lack of the furrow. This indicates that the cells are in a state of cytokinesis arrest as opposed to issues arising from proper partition, as seen by the presence of 2 nuclei but no zoids.

The nabelschnur represents the linker between two replicated kDNAs, with its process of dissolution or breakdown yet undetermined. Although TbLAP1 contains a bioinformatically predicted metalloprotease domain, its ablation suggests that this protein does not participate in cleaving of the nabelschnur, evidenced by successfully separated kDNA discs (whether the predicted active site is catalytically functional remains unknown, with the possibility of LAP1 being a pseudoprotease). Furthermore, TbLAP1 shows greatest expression in the late G_1 phase, with a notable decrease in the S phase (Figure S4). While the depletion of TbLAP1 mRNA was not as absolute as that demonstrated for TbNAB70 in the present study,[9] together this suggests that TbLAP1 is sequentially active before TbNAB70 and does not mediate nabelschnur dissolution.

Of the kDNA replication machinery and TAC complexes, only TAP110 and Tb927.11.6660 showed notable upregulation. TAP110 overexpression was previously shown to result in upregulation of Tb927.11.6660,[16] suggesting an uncharacterized interaction between the two. TAP110 has also been proposed as a kDNA segregation factor, with Tb927.11.6660 potentially providing a conduit for mitochondrial-nuclear communication,[16] although neither of these proteins localize to the nabelschnur, suggesting an indirect role in segregation. We propose that TAP110 and Tb927.11.6660 upregulation following TbNAB70 depletion represents a compensatory response to segregation difficulties encountered post replication of kDNA. While expression levels of both proteins resemble patterns of TbNAB70, they ultimately show maximal expression in the G_2/M phase (Figure S4). As we do not observe enrichment of other G_2/M peak expression sequences following TbNAB70 depletion, it is unlikely that this accumulation is strictly the result of cell-cycle arrest in the S phase. While mass spectrometry data for TAP110 overexpression are not publicly available,[16] we remain curious as to whether TbNAB70 levels were affected in this study. POLIC, the only notably depleted replication component, additionally participates in proper kDNA positioning prior to separation, referred to as the "bridge" between replication and segregation processes.[27] POLIC accumulates at the APSs during S phase, to which our data suggest a dependency on TbNAB70 for successful recruitment.

Based on their phylogenetic distribution, *TbLAP1* and *Tb927.11.6660* preceded the development of kDNA and likely represent proteins repurposed or adapted to mediate processes associated with this unique structure. By contrast, *TbNAB70* and *TAP110* superseded the emergence of this complex and evolutionarily improbable structure.[28] These two genes seemingly appeared in tandem, and we speculate that the encoded proteins may have fulfilled the functional requirements of an increasingly complex organelle substructure that is already known to mandate dozens of proteins for its maintenance.[3,29] Based on our survey of gene conservation, *N. esmeraldas* may provide complementary insight on the function of these proteins, having lost both "recent" additions of *TbNAB70* and *TAP110*, combined with its recently established tractability to investigate and potentially re-introduce specific genes of interest.[30,31] Coincidently, we also note that two of three surveyed flagellates that have specifically lost *TbNAB70* and/or *TAP110* also bear bacterial endosymbionts, such acquisitions representing a comparatively rare occurrence among trypanosomatids.[32] Whether a causative relationship exists between these two events remains an exciting possibility to be explored.

Although TbNAB70 is confined to the obligatory parasitic kinetoplastids, we found hits to various mitochondrial-DNA-binding proteins containing HMG boxes, domains known to interact with high affinity to non-B-type DNA, such as kinked, bent, or unwound DNA, during the replication process.[20] A previously described kDNA constituent, TbKAP6, has been shown to contain a single HMG box domain, with its depletion resulting in a loss of minicircles and maxicircles, while overexpression led to an increase of decatenated minicircles.[33] TbKAP6 was not affected in our depletome analysis but, considering our findings affecting kDNA catenation, it remains a possibility that TbNAB70 represents a complementary counterpart to TbKAP6, reattaching minicircles released via TbKAP6. Given that nicked and gapped minicircles as well as maxicircles are observed during kDNA segregation itself, with nicked maxicircles forming the final thread-like structure consistent with the nabelschnur,[7] TbNAB70's co-localization may also suggest a role in final repair of maxicircles during completion of segregation.

Our work suggests that during and/or after kDNA replication, TbNAB70 interacts with the kDNA mediating the separation of the daughter networks, possibly through the reattachment of released kDNA and/or recruitment of other relevant proteins, forming the nabelschnur in this process. Following the depletion of TbNAB70, the basal bodies are typically unable to segregate (and perhaps rotate) in the absence of divided kDNA and, as a result, new flagellum elongation is stalled, comparatively depleting the FAZ components as well as SAS6 (Figures 2H, 2I, and S3), a protein associated with basal body stability and flagellum assembly,[34] ultimately arresting cytokinesis (Figure 4). Although our findings strongly support the view of a nabelschnur-mediated kDNA segregation mechanism dependent on TbNAB70, other components of this enigmatic structure may remain undiscovered. In conclusion, the identification of TbNAB70 sheds light on the mechanisms of kDNA segregation and thus fulfills the criteria for a regulatory component of the nabelschnur, critical for the successful partitioning of kDNA, long-presumed to exist but hypothetical until now.

RESOURCE AVAILABILITY

Lead contact

Further information and requests for resources and reagents should be directed to and will be fulfilled by the lead contact, Lawrence Rudy Cadena (Lawrence.Cadena@hhu.de).

Materials availability

The TbNAB70-V5:TbNAB70-RNAi cell line and all antibodies utilized in this paper are available from either the lead contact or Michael Hammond (michael.hammond@paru.cas.cz) upon request.

Data and code availability

- The mass spectroscopy data have been deposited to the ProteomeXchange Consortium (http://www.proteomexchange.org) via the PRIDE partner repository with the dataset identifier PXD050771.
- This paper does not report original code.
- Any additional information required to reanalyze the data reported in this paper is available from the lead contact upon request.

ACKNOWLEDGMENTS

We thank Karel Harant and Pavel Talacko (Charles University, Prague) for performing LC-MS/MS analysis and Ken Stuart (Seattle Children's Research Institute, Seattle) for the HSP70 antibody. We are grateful to Keith Gull (University of Oxford) for fruitful discussions and for the FAZ and YL1/2 antibodies. We also thank Hassan Hashimi (Institute of Parasitology, Czech Academy of Sciences) for methodological discussions. We acknowledge support from the Czech Science Foundation 22-01026S (to V.Y.) and 22-14356S (to J.L.), EU's Operational Program "Just Transition" CZ.22_003/0000003 LERCO (to V.Y.), and Czech BioImaging grant LM2015062 (to M.T.).

AUTHOR CONTRIBUTIONS

Conceptualization: L.R.C. and J.L.; methodology: L.R.C., M.H., M.T., Ľ.C., M.S., and I.M.D.; validation: L.R.C. and M.H.; formal analysis: L.R.C. and M.H.; investigation: L.R.C. and M.H.; resources: J.L. and V.Y.; writing – original draft: L.R.C., M.H., and J.L.; writing – review & editing: L.R.C., M.H., V.Y., and J.L.; visualization: L.R.C. and M.H.; supervision: J.L.; project administration: J.L.; funding acquisition: J.L. and V.Y.

DECLARATION OF INTERESTS

The authors declare no competing interests.

STAR★METHODS

Detailed methods are provided in the online version of this paper and include the following:

- KEY RESOURCES TABLE
- EXPERIMENTAL MODEL AND SUBJECT DETAILS
  - Generation of *T. brucei* transgenic cell lines
  - Cell culturing
- METHOD DETAILS
  - Immunofluorescence microscopy
  - Transmission electron microscopy and immunogold labeling
  - Western blot
  - Southern-blot quantification of maxicircle and minicircles abundance
  - Protein preparation and mass spectroscopy
  - Analysis of mass spectrometry peptides
  - *In silico* structural analysis
  - Conservation and synteny survey
- QUANTIFICATION AND STATISTICAL ANALYSIS

SUPPLEMENTAL INFORMATION

Supplemental information can be found online at https://doi.org/10.1016/j.cub.2024.08.044.

Received: April 13, 2024
Revised: July 17, 2024
Accepted: August 23, 2024
Published: September 24, 2024

REFERENCES

1. Lane, N., and Martin, W. (2010). The energetics of genome complexity. Nature *467*, 929–934. https://doi.org/10.1038/nature09486.
2. Raval, P.K., Garg, S.G., and Gould, S.B. (2022). Endosymbiotic selective pressure at the origin of eukaryotic cell biology. eLife *11*, e81033. https://doi.org/10.7554/eLife.81033.
3. Jensen, R.E., and Englund, P.T. (2012). Network news: The replication of kinetoplast DNA. Annu. Rev. Microbiol. *66*, 473–491. https://doi.org/10.1146/annurev-micro-092611-150057.
4. Wheeler, R.J., Gull, K., and Sunter, J.D. (2019). Coordination of the cell cycle in trypanosomes. Annu. Rev. Microbiol. *73*, 133–154. https://doi.org/10.1146/annurev-micro-020518-115617.
5. Amodeo, S., Bregy, I., and Ochsenreiter, T. (2023). Mitochondrial genome maintenance—the kinetoplast story. FEMS Microbiol. Rev. *47*, https://doi.org/10.1093/femsre/fuac047.
6. Aeschlimann, S., Stettler, P., and Schneider, A. (2023). DNA segregation in mitochondria and beyond: insights from the trypanosomal tripartite attachment complex. Trends Biochem. Sci. *48*, 1058–1070. https://doi.org/10.1016/j.tibs.2023.08.012.
7. Gluenz, E., Povelones, M.L., Englund, P.T., and Gull, K. (2011). The kinetoplast duplication cycle in *Trypanosoma brucei* is orchestrated by cytoskeleton-mediated cell morphogenesis. Mol. Cell. Biol. *31*, 1012–1021. https://doi.org/10.1128/MCB.01176-10.
8. Gluenz, E., Shaw, M.K., and Gull, K. (2007). Structural asymmetry and discrete nucleic acid subdomains in the *Trypanosoma brucei* kinetoplast. Mol. Microbiol. *64*, 1529–1539. https://doi.org/10.1111/j.1365-2958.2007.05749.x.
9. Peña-Diaz, P., Vancová, M., Resl, C., Field, M.C., and Lukeš, J. (2017). A leucine aminopeptidase is involved in kinetoplast DNA segregation in *Trypanosoma brucei*. PLoS Pathog. *13*, e1006310. https://doi.org/10.1371/journal.ppat.1006310.
10. Pyrih, J., Hammond, M., Alves, A., Dean, S., Sunter, J.D., Wheeler, R.J., Gull, K., and Lukeš, J. (2023). Comprehensive sub-mitochondrial protein map of the parasitic protist *Trypanosoma brucei* defines critical features of organellar biology. Cell Rep. *42*, 113083. https://doi.org/10.1016/j.celrep.2023.113083.
11. Poon, S.K., Peacock, L., Gibson, W., Gull, K., and Kelly, S. (2012). A modular and optimized single marker system for generating *Trypanosoma brucei* cell lines expressing T7 RNA polymerase and the tetracycline repressor. Open Biol. *2*, 110037. https://doi.org/10.1098/rsob.110037.
12. Dean, S., Sunter, J., Wheeler, R.J., Hodkinson, I., Gluenz, E., and Gull, K. (2015). A toolkit enabling efficient, scalable and reproducible gene tagging in trypanosomatids. Open Biol. *5*, 140197. https://doi.org/10.1098/rsob.140197.
13. McAllaster, M.R., Sinclair-Davis, A.N., Hilton, N.A., and de Graffenried, C.L. (2016). A unified approach towards *Trypanosoma brucei* functional genomics using Gibson assembly. Mol. Biochem. Parasitol. *210*, 13–21. https://doi.org/10.1016/j.molbiopara.2016.08.001.
14. Concepción-Acevedo, J., Miller, J.C., Boucher, M.J., and Klingbeil, M.M. (2018). Cell cycle localization dynamics of mitochondrial DNA polymerase IC in African trypanosomes. Mol. Biol. Cell *29*, 2540–2552. https://doi.org/10.1091/mbc.E18-02-0127.
15. Klingbeil, M.M., Motyka, S.A., and Englund, P.T. (2002). Multiple mitochondrial DNA polymerases in *Trypanosoma brucei*. Mol. Cell *10*, 175–186. https://doi.org/10.1016/S1097-2765(02)00571-3.
16. Amodeo, S., Kalichava, A., Fradera-Sola, A., Bertiaux-Lequoy, E., Guichard, P., Butter, F., and Ochsenreiter, T. (2021). Characterization of the novel mitochondrial genome segregation factor TAP110 in *Trypanosoma brucei*. J. Cell Sci. *134*, jcs254300. https://doi.org/10.1242/jcs.254300.
17. Schimanski, B., Aeschlimann, S., Stettler, P., Käser, S., Gomez-Fabra Gala, M., Bender, J., Warscheid, B., Vögtle, F.-N., and Schneider, A.

(2022). p166 links membrane and intramitochondrial modules of the trypanosomal tripartite attachment complex. PLoS Pathog. *18*, e1010207. https://doi.org/10.1371/journal.ppat.1010207.

18. Aphasizheva, I., Maslov, D.A., Qian, Y., Huang, L., Wang, Q., Costello, C.E., and Aphasizhev, R. (2016). Ribosome-associated pentatricopeptide repeat proteins function as translational activators in mitochondria of trypanosomes. Mol. Microbiol. *99*, 1043–1058. https://doi.org/10.1111/mmi.13287.
19. Tarrés-Solé, A., Battistini, F., Gerhold, J.M., Piétrement, O., Martínez-García, B., Ruiz-López, E., Lyonnais, S., Bernadó, P., Roca, J., Orozco, M., et al. (2023). Structural analysis of the Candida albicans mitochondrial DNA maintenance factor Gcf1p reveals a dynamic DNA-bridging mechanism. Nucleic Acids Res. *51*, 5864–5882. https://doi.org/10.1093/nar/gkad397.
20. Štros, M., Launholt, D., and Grasser, K.D. (2007). The HMG-box: a versatile protein domain occurring in a wide variety of DNA-binding proteins. Cell. Mol. Life Sci. *64*, 2590–2606. https://doi.org/10.1007/s00018-007-7162-3.
21. Malarkey, C.S., and Churchill, M.E.A. (2012). The high mobility group box: the ultimate utility player of a cell. Trends Biochem. Sci. *37*, 553–562. https://doi.org/10.1016/j.tibs.2012.09.003.
22. Antonietti, M., Gonzalez, D.J.T., Djulbegovic, M., Dayhoff, G.W., Uversky, V.N., Shields, C.L., and Karp, C.L. (2023). Intrinsic disorder in PRAME and its role in uveal melanoma. Cell Commun. Signal. *21*, 222. https://doi.org/10.1186/s12964-023-01197-y.
23. Kostygov, A.Y., Karnkowska, A., Votýpka, J., Tashyreva, D., Maciszewski, K., Yurchenko, V., and Lukeš, J. (2021). Euglenozoa: taxonomy, diversity and ecology, symbioses and viruses. Open Biol. *11*, 200407. https://doi.org/10.1098/rsob.200407.
24. Archer, S.K., Inchaustegui, D., Queiroz, R., and Clayton, C. (2011). The cell cycle regulated transcriptome of *Trypanosoma brucei*. PLoS One *6*, e18425. https://doi.org/10.1371/journal.pone.0018425.
25. Kohl, L., Robinson, D., and Bastin, P. (2003). Novel roles for the flagellum in cell morphogenesis and cytokinesis of trypanosomes. EMBO J. *22*, 5336–5346. https://doi.org/10.1093/emboj/cdg518.
26. Shi, J., Franklin, J.B., Yelinek, J.T., Ebersberger, I., Warren, G., and He, C.Y. (2008). Centrin4 coordinates cell and nuclear division in *T. brucei*. J. Cell Sci. *121*, 3062–3070. https://doi.org/10.1242/jcs.030643.
27. Miller, J.C., Delzell, S.B., Concepción-Acevedo, J., Boucher, M.J., and Klingbeil, M.M. (2020). A DNA polymerization-independent role for mitochondrial DNA polymerase I-like protein C in African trypanosomes. J. Cell Sci. *133*, jcs233072.. https://doi.org/10.1242/jcs.233072.
28. Lukeš, J., Guilbride, D.L., Votýpka, J., Zíková, A., Benne, R., and Englund, P.T. (2002). Kinetoplast DNA network: Evolution of an improbable structure. Eukaryot. Cell *1*, 495–502. https://doi.org/10.1128/EC.1.4.495-502.2002.
29. Povelones, M.L. (2014). Beyond replication: division and segregation of mitochondrial DNA in kinetoplastids. Mol. Biochem. Parasitol. *196*, 53–60. https://doi.org/10.1016/j.molbiopara.2014.03.008.
30. Zakharova, A., Saura, A., Butenko, A., Podešvová, L., Warmusová, S., Kostygov, A.Y., Nenarokova, A., Lukeš, J., Opperdoes, F.R., and Yurchenko, V. (2021). A new model Trypanosomatid, *Novymonas esmeraldas*: Genomic perception of its "Candidatus Pandoraea novymonadis" Endosymbiont. mBio *12*, e0160621. https://doi.org/10.1128/mBio.01606-21.
31. Zakharova, A., Tashyreva, D., Butenko, A., Morales, J., Saura, A., Svobodová, M., Poschmann, G., Nandipati, S., Zakharova, A., Noyvert, D., et al. (2023). A neo-functionalized homolog of host transmembrane protein controls localization of bacterial endosymbionts in the trypanosomatid *Novymonas esmeraldas*. Curr. Biol. *33*, 2690–2701.e5. https://doi.org/10.1016/j.cub.2023.04.060.
32. Harmer, J., Yurchenko, V., Nenarokova, A., Lukeš, J., and Ginger, M.L. (2018). Farming, slaving and enslavement: histories of endosymbioses during kinetoplastid evolution. Parasitology *145*, 1311–1323. https://doi.org/10.1017/S0031182018000781.
33. Wang, J., Pappas-Brown, V., Englund, P.T., and Jensen, R.E. (2014). TbKAP6, a mitochondrial HMG box-containing protein in *Trypanosoma brucei*, is the first Trypanosomatid kinetoplast-associated protein essential for kinetoplast DNA replication and maintenance. Eukaryot. Cell *13*, 919–932. https://doi.org/10.1128/EC.00260-13.
34. Hu, H., Liu, Y., Zhou, Q., Siegel, S., and Li, Z. (2015). The centriole cartwheel protein SAS-6 in *Trypanosoma brucei* is required for probasal body biogenesis and flagellum assembly. Eukaryot. Cell *14*, 898–907. https://doi.org/10.1128/EC.00083-15.
35. Sherwin, T., Schneider, A., Sasse, R., Seebeck, T., and Gull, K. (1987). Distinct localization and cell cycle dependence of COOH terminally tyrosinolated alpha-tubulin in the microtubules of *Trypanosoma brucei brucei*. J. Cell Biol. *104*, 439–446. https://doi.org/10.1083/jcb.104.3.439.
36. Vaughan, S., Kohl, L., Ngai, I., Wheeler, R.J., and Gull, K. (2008). A repetitive protein essential for the flagellum attachment zone filament structure and function in *Trypanosoma brucei*. Protist *159*, 127–136. https://doi.org/10.1016/j.protis.2007.08.005.
37. Cadena, L.R., Gahura, O., Panicucci, B., Zíková, A., and Hashimi, H. (2021). Mitochondrial contact site and cristae organization system and F_1F_O-ATP synthase crosstalk is a fundamental property of mitochondrial cristae. mSphere *6*, e0032721. https://doi.org/10.1128/mSphere.00327-21.
38. Wickstead, B., Ersfeld, K., and Gull, K. (2002). Targeting of a tetracycline-inducible expression system to the transcriptionally silent minichromosomes of *Trypanosoma brucei*. Mol. Biochem. Parasitol. *125*, 211–216. https://doi.org/10.1016/s0166-6851(02)00238-4.
39. Redmond, S., Vadivelu, J., and Field, M.C. (2003). RNAit: an automated web-based tool for the selection of RNAi targets in *Trypanosoma brucei*. Mol. Biochem. Parasitol. *128*, 115–118. https://doi.org/10.1016/S0166-6851(03)00045-8.
40. Schneider, C.A., Rasband, W.S., and Eliceiri, K.W. (2012). NIH image to ImageJ: 25 years of image analysis. Nat. Methods *9*, 671–675. https://doi.org/10.1038/nmeth.2089.
41. Pérez-Morga, D., and Englund, P.T. (1993). The structure of replicating kinetoplast DNA networks. J. Cell Biol. *123*, 1069–1079.
42. Cox, J., Hein, M.Y., Luber, C.A., Paron, I., Nagaraj, N., and Mann, M. (2014). Accurate proteome-wide label-free quantification by delayed normalization and maximal peptide ratio extraction, termed MaxLFQ. Mol. Cell. Proteomics *13*, 2513–2526. https://doi.org/10.1074/mcp.M113.031591.
43. Zimmermann, L., Stephens, A., Nam, S.-Z., Rau, D., Kübler, J., Lozajic, M., Gabler, F., Söding, J., Lupas, A.N., and Alva, V. (2018). A completely reimplemented MPI bioinformatics toolkit with a new HHpred server at its core. J. Mol. Biol. *430*, 2237–2243. https://doi.org/10.1016/j.jmb.2017.12.007.
44. Necci, M., Piovesan, D., Dosztányi, Z., and Tosatto, S.C.E. (2017). MobiDB-lite: fast and highly specific consensus prediction of intrinsic disorder in proteins. Bioinformatics *33*, 1402–1404. https://doi.org/10.1093/bioinformatics/btx015.
45. Nielsen, H. (2017). Predicting secretory proteins with SignalP. Methods Mol. Biol. *1611*, 59–73. https://doi.org/10.1007/978-1-4939-7015-5_6.
46. Jumper, J., Evans, R., Pritzel, A., Green, T., Figurnov, M., Ronneberger, O., Tunyasuvunakool, K., Bates, R., Žídek, A., Potapenko, A., et al. (2021). Highly accurate protein structure prediction with AlphaFold. Nature *596*, 583–589. https://doi.org/10.1038/s41586-021-03819-2.
47. Albanaz, A.T.S., Carrington, M., Frolov, A.O., Ganyukova, A.I., Gerasimov, E.S., Kostygov, A.Y., Lukeš, J., Malysheva, M.N., Votýpka, J., Zakharova, A., et al. (2023). Shining the spotlight on the neglected: new high-quality genome assemblies as a gateway to understanding the evolution of Trypanosomatidae. BMC Genomics *24*, 471. https://doi.org/10.1186/s12864-023-09591-z.

STAR★METHODS

KEY RESOURCES TABLE

REAGENT or RESOURCE	SOURCE	IDENTIFIER
Antibodies		
Mouse anti-V5	Thermo Fisher Scientific	Catalog #: 377500; RRID: AB_2533339
Alexa Fluor 488 goat anti-mouse IgG	Invitrogen / Thermo Fisher Scientific	Catalog #: A28175; RRID: AB_2536161
Rat anti-YL1/2	Sherwin et al.[35]	N/A
Rat anti-L3B2	Vaughan et al.[36]	N/A
Mouse anti-HSP70	See acknowledgments	N/A
Critical commercial assays		
Human T Cell Nucleofector Kit, 100 reactions	Lonza	Catalog #: R2050
DIG Easy Hyb	Roche	Catalog #: 11603558001
Deposited data		
HHPred output	See Table S1	N/A
Ortholog sequences	See Table S2	N/A
TbNAB70 depletome MS^2 data	PRIDE	PXD050771
TbNAB70 AlphaFold2 structure	AlphaFold Protein Structure Database	AF-Q384P8-F1
Experimental models: Cell lines		
TbNAB70-V5:TbNAB70 ↓	This study	N/A
Experimental models: Organisms/strains		
Trypanosoma brucei SmOxP927	Poon et al.[11] and Dean et al.[12]	RRID: SCR_004786
Oligonucleotides		
For oligonucleotides used in this study, see Table S3	N/A	N/A
Recombinant DNA		
pPOTv4-HygR	Dean et al.[12] and Cadena et al.[37]	N/A
p2T7-177	Wickstead et al.[38]	N/A
Software and algorithms		
GraphPad Prism 7	GraphPad	https://www.graphpad.com/
Image Lab	Bio-Rad	https://bio-rad.com/en-de/product/image-lab-software?ID=KRE6P5E8Z
AlphaFold2 v1.5.5	Colab	https://colab.research.google.com/github/sokrypton/ColabFold/blob/main/AlphaFold2.ipynb
ImageJ	National Institutes of Health	https://imagej.net/ij/index.html

EXPERIMENTAL MODEL AND SUBJECT DETAILS

Generation of *T. brucei* transgenic cell lines

Trypanosoma brucei SmOxP927 procyclic cell line[11,12] was transfected by electroporation using the Amaxa apparatus (Lonza) set with the program X-14. After transfection, cells were seeded in 24-well plates in serial dilutions and selected by the appropriate resistance marker. For endogenous $V5_{\times 3}$ epitope, a previously described strategy was employed.[12] Briefly, C-terminus endogenous tagging amplicons were obtained using long primers targeting a modified pPOTv4 vector containing a $V5_{\times 3}$ epitope. Cells were selected with Hygromycin (Thermo Fisher Scientific) at 50 μg/ml and screened for V5 expression by western blotting. For generation of the RNAi cell line, PCR products targeting a specific CDC region as determined by RNAit[39] were cloned into the p2T7-177 vector.[38] *Not*I-linearized construct was electroporated using the same conditions as above into the $V5_{\times 3}$ tagged cell line. Cells were selected with Phleomycin (Sigma-Aldrich / Merck) at 2.5 μg/ml. Knockdown of the protein was monitored by western blotting against the $V5_{\times 3}$ epitope using α-V5 mouse primary antibody (Invitrogen / Thermo Fisher Scientific – 1:1000). Oligonucleotides used for PCR amplification are given in Table S3.

Cell culturing

Cells were grown at 27°C in SDM-79 medium supplemented with 10 % fetal bovine serum and 7.5 mg/l hemin. Cells were grown in the presence and absence of 1 μg/ml tetracycline (Sigma-Aldrich / Merck) for RNAi induction. Cell density was measured using the Beckman Coulter Z2 cell and particle counter (Beckman Coulter) and maintained at the exponential mid-log growth phase throughout the analysis.

METHOD DETAILS

Immunofluorescence microscopy

A total of 10^6 *T. brucei* cells were fixed with 4 % paraformaldehyde for 30 min at room temperature (RT). The cells were subsequently centrifuged at 1,300 × g for 5 min, resuspended in 200 μl 1 × PBS, and placed on a glass slide for 30 min. The slides were washed with PBS and allowed to permeabilize in methanol for 30 min at -20°C. The slides were washed thrice with PBS and blocked with 5 % milk inside a humid chamber for 1 h before being incubated with α-V5 mouse primary antibody (Thermo Fisher Scientific – 1:400) overnight at 4°C. The slides were washed once again with PBS and incubated with secondary Alexa Fluor 488 goat α-mouse IgG antibody (Invitrogen / Thermo Fisher Scientific – 1:1,000) for 1 h at RT. The slides were washed with PBS before a final wash with water, air-dried, and mounted in ProLong Gold antifade reagent DAPI (Invitrogen / Thermo Fisher Scientific). Images were captured with the BX51 Fluorescence Microscope (Olympus). For Mitotracker Red staining (Invitrogen / Thermo Fisher Scientific), the same procedure was performed with the exception of incubating cells in culture with the staining 30 min prior to fixation. Fluorescent intensity analysis was performed using ImageJ.[40]

Mature basal bodies were illuminated as above with monoclonal rat antibody YL1/2, specific to tyrosinated tubulin (1:500)[35] followed by secondary Alexa Fluor 488 goat α-mouse IgG antibody (Invitrogen / Thermo Fisher Scientific – 1:100). FAZ was visualized *via* anti-FAZ1 antibody L3B2 (antigenic to Tb927.4.3740, 1:3)[36] followed by secondary Alexa Fluor 488 goat α-mouse IgG antibody (Invitrogen / Thermo Fisher Scientific – 1:1,000). 64 and 52 1K2N cells were counted to quantitate detached flagella and mature basal body segregation, respectively.

Transmission electron microscopy and immunogold labeling

The cell pellet was fixed in a mixture of 4% formaldehyde and 0.1% glutaraldehyde in 0.1M HEPES (Sigma-Aldrich / Merck) for 1 h at RT, resuspended and washed with 0.1M HEPES, embedded into 10% gelatin (Serva Electrophoresis) and subsequently transferred into 2.3M sucrose solution for 72 h at 4 °C. Next, the pellet was cut in small gelatin blocks mounted onto flat copper stubs and plunge frozen in liquid nitrogen. Ultrathin cryosections (100 nm) were generated using a cryo-ultramicrotome (Leica) at −100 °C. The sections were picked using a drop of 1% methyl cellulose/1.05 M sucrose mixture, transferred onto a formvar-carbon coated grid, treated with blocking buffer (TEM-BB) composed of 1% fish skin gelatin (Sigma-Aldrich / Merck) dissolved in 0.1M HEPES for 1 h, and incubated with primary α-V5 monoclonal antibody (Thermo Fisher Scientific – 1:30) for 30 min at RT. After washing in TEM-BB, the sections were incubated with secondary α-protein A monoclonal antibody conjugated with gold nanoparticles (UMC Utrecht – 1:50) in TEM-BB for 30 min at RT. A control for the non-specific binding of the secondary antibody was performed by omitting the primary antibody. Finally, the cryosections were contrasted using a mixture of 2% methylcellulose and 3% aqueous uranyl acetate solution (9:1), and observed in JEOL JEM 1400-Flash at an accelerating voltage 120 kV. 20 cells of classically imaged TEM for both uninduced and 48 hours post induction lines, which displayed a visible flagella pocket, kDNA disc and two flagella and/or basal bodies had their flagella status and kDNA density examined.

Western blot

Whole cell lysate from 10^6 *T. brucei* cells were loaded onto an SDS-PAGE gel and transferred to a PVDF membrane. Membranes were probed with either anti-V5 mouse primary antibody (Invitrogen / Thermo Fisher Scientific – 1:4,000) or α-HSP70 primary antibody (see Acknowledgements – 1:10,000) and incubated overnight at 4°C. This was followed by incubation with a secondary horseradish peroxidase-conjugated α-mouse antibody (BioRad – 1:2,000) for 1 h at RT. Proteins were visualized using the Pierce ECL system (Genetica / BioRad) on a ChemiDoc instrument (BioRad).

Southern-blot quantification of maxicircle and minicircles abundance

Total DNA was isolated from mid-log phase cultures before RNAi induction and on hours 24 and 48 post RNAi induction. The cell pellets were washed in PBS and resuspended in TRI Reagent (Molecular Research Center) as per the manufacturer's suggestions. Five μg of total DNA per lane and probe was digested with *Hind*III and *Xba*I (tubulin and maxicircles-specific probes) or *Rsa*I (minicircles-specific probes). Digested DNA was resolved on 0.75 % agarose gel and transferred to nylon membrane (Amersham). The hybridization was performed overnight using DIG Easy Hyb (Roche). Probes to detect tubulin, maxi- and minicircles were PCR amplified and labelled using PCR DIG Probe Synthesis Kit (Roche). The detection was done using DIG Luminiscent Detection Kit (Roche) following the recommendations of the manufacturer. Oligonucleotides used for PCR amplification are given in Table S3.

kDNA was isolated as described previously on a sucrose cushion[41] using 200 ml cultures harvested in mid-log phase before RNAi induction and on 48 hours post RNAi induction. 100 ng of undigested kDNA per lane was run on an 0.8% agarose gel (1 hour, 100 Volts) against a 1 kb Plus DNA ladder (Invitrogen) and visualized with ethidium bromide.

Protein preparation and mass spectroscopy

Triplicate whole cell lysates homogenized by sonication in 1% SDS were processed for mass spectroscopy analysis as described previously.[37] In brief, samples were resuspended in 100 mM tetraethylammonium bromide (TEAB) containing 2 % SDS. Cysteines were reduced with a final concentration of 10 mM Tris(2-carboxyethyl) phosphine hydrochloride (TCEP) and subsequently cleaved with 1 μg of trypsin overnight at 37°C. After digestion, 1 % trifluoroacetic acid (TFA) was added to wash twice, and samples were resuspended in 20 μl of TFA per 100 μg of protein. A non-reversed-phased column (Easp-Spray column, 50-cm by 75-μm inner diameter, PepMap C_{18}, 2-μm particles, 100-Å pore size) was used for LC-MS analysis. Mobile phase buffer A consisted of water and 0.1 % formic acid. Mobile phase B consisted of acetonitrile and 0.1 % formic acid. Samples were loaded onto the trap column (Acclaim PepMap300 C_{18}, 5 μm, 300-Å-wide pore, 300 μm by 5 mm) at a flow rate of 15 μl/min. The loading buffer consisted of water, 2 % acetonitrile, and 0.1 % TFA. Peptides were eluted using a mobile phase gradient from 2 % to 40 % over 60 min at a flow rate of 300 nl/min. The peptide cations eluted were converted to gas-phase ions *via* electrospray ionization and analyzed on a Thermo Orbitrap Fusion instrument (Q-OT-qIT – Thermo Fisher). Full MS spectra were acquired in the Orbitrap instrument with a mass range of 350 to 1,400 *m/z*, at a resolution of 120,000 at 200 *m/z*, and with a maximum injection time of 50 ms. Tandem MS was performed by isolation at 1.5 Th with the quadrupole, high-energy collisional dissociation (HCD) fragmentation with a normalized collision energy of 30, and rapid-scan MS analysis in the ion trap. The MS/MS ion count target was set to 10^4, and the maximum infection time was set at 35 ms. Only those precursors with a charge state of 2 to 6 were sampled. The dynamic exclusion duration was set to 45 s with a 10-ppm tolerance around the selected precursor and its isotopes, Monoisotopic precursor selection was on with a top-speed mode of 2-s cycles.

Analysis of mass spectrometry peptides

Label-free quantification of the data was performed using MaxQuant software (v. 1.6.2.1).[42] The false discovery rates for peptides and proteins were set to 1 % with a specified minimum peptide length of 7 amino acids. The Andromeda search engine was used for the MS/MS spectra against the *Trypanosoma brucei* database (downloaded from UniProt, December 2021, containing 8,306 entries). Enzyme specificity was set to C-terminal Arg and Lys, alongside cleavage at proline bonds, with a maximum of 2 missed cleavages. Dithiomethylation of cysteine was selected as a fixed modification, with N-terminal protein acetylation and methionine oxidation as variable modifications. The "match between runs" feature in MaxQuant was used to transfer identification to other LC-MS/MS runs based on mass and retention time with a maximum deviation of 0.7 min. Quantifications were performed using a label-free algorithm as described.[42] Data analysis was performed using Perseus software (v. 1.6.1.3).

In silico structural analysis

The regions homologous to different HMG box domain containing proteins was predicted using the HHpred toolkit (see Table S1 for list of all homologous proteins with e-scores).[43] The mitochondrial targeted signal, coiled coil domain, and intrinsic disordered domain were predicted using SignalP 4.1, Coils, and MobiDB-lite, respectively.[43–45] The predicted tertiary structure of TbNAB70 was generated using AlphaFold2[46] under the AlphaFold Protein Structure Database identifier AF-Q384P8-F1.

Conservation and synteny survey

Reciprocal BLAST searches were conducted against genes for *TbLAP1* (*Tb927.8.3060*), *TbNAB70* (*Tb927.11.7580*), *TAP110* (*Tb927.11.7590*), and *Tb927.11.6660* against a variety of publicly available Kinetoplastid, Diplonmeid, and Euglenid CDS, with a threshold E^{-5} value. Gene synteny specifically was surveyed within the genomes of Trypanosomatidae with N_{50} values of 500 kb or greater, along with *Paratrypanosoma confusum* and *Bodo saltans*.[47]

QUANTIFICATION AND STATISTICAL ANALYSIS

Figure 1C

Measurement of distance using ImageJ was recorded in ninety cells and quantified using an independent sample T-test in GraphPad Prism. See Figure 1C legend for details.

Figure 1D

Measurement of fluorescence intensity using ImageJ was recorded in forty cells and quantified using an independent sample T-test in GraphPad Prism. Maximum value (asterisks) for "present" was 2.43 units and for "absent" 1.62 units. See Figure 1D legend for details.

Figure 2G

Measurement of fluorescence intensity using ImageJ was recorded in twenty cells and quantified using an independent sample T-test in GraphPad Prism. Maximum value (asterisks) for 1K1N was 1.4 units. Maximum and minimum value (asterisks) for 1K2N was 2.28 units and 0.98 units, respectively.